Molecular Therapy
Oncolytics
Original Article

AMERICAN SOCIETY of GENE & CELL THERAPY

Fludarabine as an Adjuvant Improves Newcastle Disease Virus-Mediated Antitumor Immunity in Hepatocellular Carcinoma

Gang Meng,[1,2] Ziwei Fei,[1] Mingyue Fang,[1] Binghua Li,[1,2] Anxian Chen,[1] Chun Xu,[1,4] Mao Xia,[3] Decai Yu,[2] and Jiwu Wei[1]

[1]Jiangsu Key Laboratory of Molecular Medicine, Medical School of Nanjing University, Nanjing 210093, China; [2]Department of Hepatobiliary Surgery, the Affiliated Drum Tower Hospital, Medical School of Nanjing University, Nanjing 210008, China; [3]Department of Clinical Laboratory, the Affiliated Drum Tower Hospital, Medical School of Nanjing University, Nanjing 210008, China; [4]Department of Pathology and Pathophysiology, Medical School, Southeast University, Nanjing 210009, China

In addition to direct oncolysis, oncolytic viruses (OVs) also induce antitumor immunity, also called viro-immunotherapy. Limited viral replication and immune-negative feedback are the major hurdles to effective viro-immunotherapy. In this study, we found that use of an adjuvant of fludarabine, a chemotherapeutic drug for chronic myeloid leukemia, increased the replication of Newcastle disease virus (NDV) by targeting signal transducer and activator of transcription 1 (STAT1), which led to enhanced oncolysis of hepatocellular carcinoma (HCC) cells. Moreover, fludarabine accelerated ubiquitin-proteasomal degradation by enhancing ubiquitylation rather than proteasomal activity. This resulted in accelerated degradation of phosphorylated STAT3 and indoleamine 2, 3-dioxygenase 1 (IDO1), whose expression was induced by NDV infection. In addition, fludarabine significantly increased the NDV-induced infiltration of NK cells and decreased the number of NDV-induced myeloid-derived suppressor cells (MDSCs) in the tumor microenvironment. The aforementioned effects of fludarabine significantly improved NDV-mediated antitumor immunity and prolonged survival in mouse model of HCC. Our findings indicate the utility of fludarabine as an adjuvant for oncolytic anticancer viro-immunotherapy.

INTRODUCTION

Oncolytic virotherapy is a highly promising treatment modality that uses replication-competent viruses to destroy cancers. The approved oncolytic virus T-VEC, a genetically engineered herpes simplex virus-1 (HSV-1) expressing granulocyte-macrophage colony-stimulating factor (GM-CSF), also known as OncoVEX^{GM-CSF}, is a milestone in viro-immunotherapy.[1] Therapeutic oncolytic viruses (OVs) activate antitumor immune responses by inducing immunogenic cell death and type I interferon (IFN)-mediated lymphocyte infiltration.[2–5] Clinical trials of various OVs such as adenovirus, vaccinia, herpesvirus, reovirus, and paramyxovirus (measles virus and Newcastle disease virus [NDV]) in advanced cancer patients have shown promise.[6]

NDV is a member of the *Avulavirus* genus of the *Paramyxoviridae* family. In both preclinical and clinical studies, NDV induced the production of type I IFNs and is an effective oncolytic agent with a good safety record.[7–9] On one hand, NDV induces both extrinsic and intrinsic apoptosis of malignant cells,[10] and on the other hand, NDV infection elicits both innate and adaptive antiviral immunity, resulting in cross-activated antitumor immune responses.[11,12] Localized therapy with oncolytic NDV induces an inflammatory response, leading to lymphocyte ($NK1.1^+$, $CD3^+CD8^+$, and $CD11b^+$ lymphocytes, and monocytes) infiltration and an antitumor effect in distant (nonvirally injected) tumors without dissemination of the virus. The therapeutic efficacy of NDV depends on $CD8^+$ T cells, natural killer (NK) cells and type I IFNs, but not $CD4^+$ lymphocytes.[13,14]

Limited viral replication and immune-negative feedback in the tumor microenvironment (TME) limit the efficacy of viro-immunotherapy for cancer. NDV is an enveloped negative-sense single-strand RNA virus[7] that elicits an antiviral innate immune response via retinoic acid-induced gene I (RIG-I) signaling, which induces the production of type I IFNs and pro-inflammatory cytokines. Signal transducer and activator of transcription 1 (STAT1) amplifies the RIG-I-mediated IFN response to RNA viruses. Several viruses (e.g., hepatitis C virus, simian virus 5, and measles virus) interfere with STAT1 phosphorylation, thereby reducing type I IFN production, which benefits viral replication.[15–17]

Antitumor immune activation is often accompanied by immune-negative feedback, including the production of immunosuppressive cytokines, cell types, and negative co-stimulators. STAT3 plays a key role in generating an immunosuppressive TME by regulating inflammation and various immune cell types including myeloid-derived suppressor cells (MDSCs), regulatory T cells (Tregs), and

Received 13 March 2019; accepted 21 March 2019;
https://doi.org/10.1016/j.omto.2019.03.004.

Correspondence: Jiwu Wei, Jiangsu Key Laboratory of Molecular Medicine, Medical School of Nanjing University, 22 Hankou Road, Nanjing, 210093, China.
E-mail: wjw@nju.edu.cn

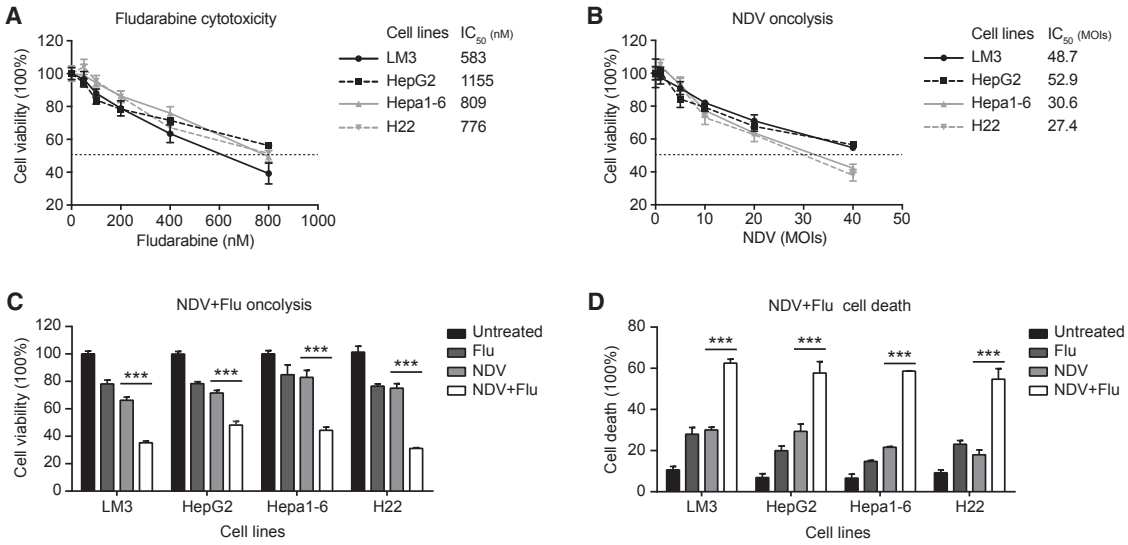

Figure 1. Fludarabine Enhances the Oncolytic Effects of NDV in HCC Cells

(A and B) LM3, HepG2, Hepa1-6, and H22 cells were seeded in 96-well plates and treated with (A) fludarabine at 0, 50, 100, 200, 400, or 800 nM or (B) infected with NDV at various MOIs of 0, 5, 10, 20, or 40 for 48 h. Cell viability was assessed by the MTT assay. Means + SDs of quadruplicates and IC_{50} (half maximal inhibitory concentration) values of fludarabine or NDV are depicted. (C and D) Cells were infected with NDV (MOI = 10) in the presence or absence of fludarabine (200 nM) for 48 h and oncolytic effects were determined by (C) the MTT assay and (D) trypan-blue exclusion assay. Means + SDs of quadruplicates are shown. ***$p < 0.001$.

T helper 17 cells (Th17).[18–20] Hyperactivation of STAT3 signaling occurs in the majority of human cancers and is correlated with a poor prognosis.[21] STAT3 activation is mediated by various cytokines (e.g., interleukin-6 [IL-6], IL-10, and IFNs). Viral infection with, for example, hepatitis C virus, Epstein-Barr virus, and varicella-zoster virus, can activate the STAT3 signaling pathway in host cells.[22] Whether NDV activates STAT3 in hepatocellular carcinoma (HCC) cells is unknown.

Metabolic changes in the TME determine the fate of immune cells such as survival, proliferation, polarization, and activities.[23,24] Indoleamine 2,3-dioxygenase 1 (IDO1) is highly expressed by dendritic cells, macrophages, MDSCs, and tumor cells and catabolizes the essential amino acid tryptophan into kynurenine. Deprivation of tryptophan and accumulation of kynurenine and its metabolic product 3-hydroxyanthranilic acid lead to apoptosis or dysfunction of effector T cells and induction of Tregs, respectively.[25–27] In some tumors, including those of the prostate, breast, brain, and blood, IDO1 is constitutively expressed and contributes to cancer-associated immune suppression.[26,28] IDO1 can be elicited by inflammatory factors, such as IFNs,[26,28] or viral infection, such as measles virus and hepatitis C virus,[29,30] and reduces the intensity of potentially deleterious immune responses. Clinical trials of IDO1 inhibitors, including indoximod, epacadostat, and NLG919 for multiple oncology indications are currently underway.[26,31]

Fludarabine is a purine analog used to treat leukemia and lymphoma that inhibits DNA synthesis by interfering with ribonucleotide reductase and DNA polymerase.[32] Fludarabine is an inhibitor of STAT1, which prevents overproduction of type I IFNs.[33] Moreover, fludarabine decreases IDO in malignant cells by proteasome-mediated degradation.[34] We and another group found that fludarabine reduces IDO1 expression therefore enhances the antitumor activity of adoptive T cells.[30,35] It is yet unknown if fludarabine downregulates STAT3 signaling. Effective antitumor immunotherapy requires both immune activation and prevention of immunosuppression. Given its multiple functions, we hypothesized that fludarabine would be a powerful adjuvant for oncolytic viro-immunotherapy. In this study, we employed oncolytic NDV to activate antitumor immunity and used fludarabine as an adjuvant to enhance NDV replication and prevent concomitant immunosuppression in HCC.

RESULTS

Fludarabine Enhances NDV-Mediated Oncolysis in HCC Cells

Fludarabine and NDV had dose-dependent cytotoxic effects on human and murine HCC cells (Figures 1A and 1B). Indeed, 200 nM fludarabine together with NDV at an MOI of 10 resulted in slight cytotoxic effects. Fludarabine dramatically enhanced the NDV-induced oncolysis of HCC cells (Figures 1C and 1D). Moreover, fludarabine and NDV significantly increased the number of annexin V-positive (apoptotic) cells (Figure S1), which indicates that fludarabine markedly enhances NDV-induced apoptotic cell death. Therefore, fludarabine significantly enhances the NDV-mediated oncolysis of HCC cells.

Fludarabine Promotes NDV Replication by Inhibiting STAT1

Next, we quantified NDV replication by determining the viral production and the expression levels of *Ndv-hn*

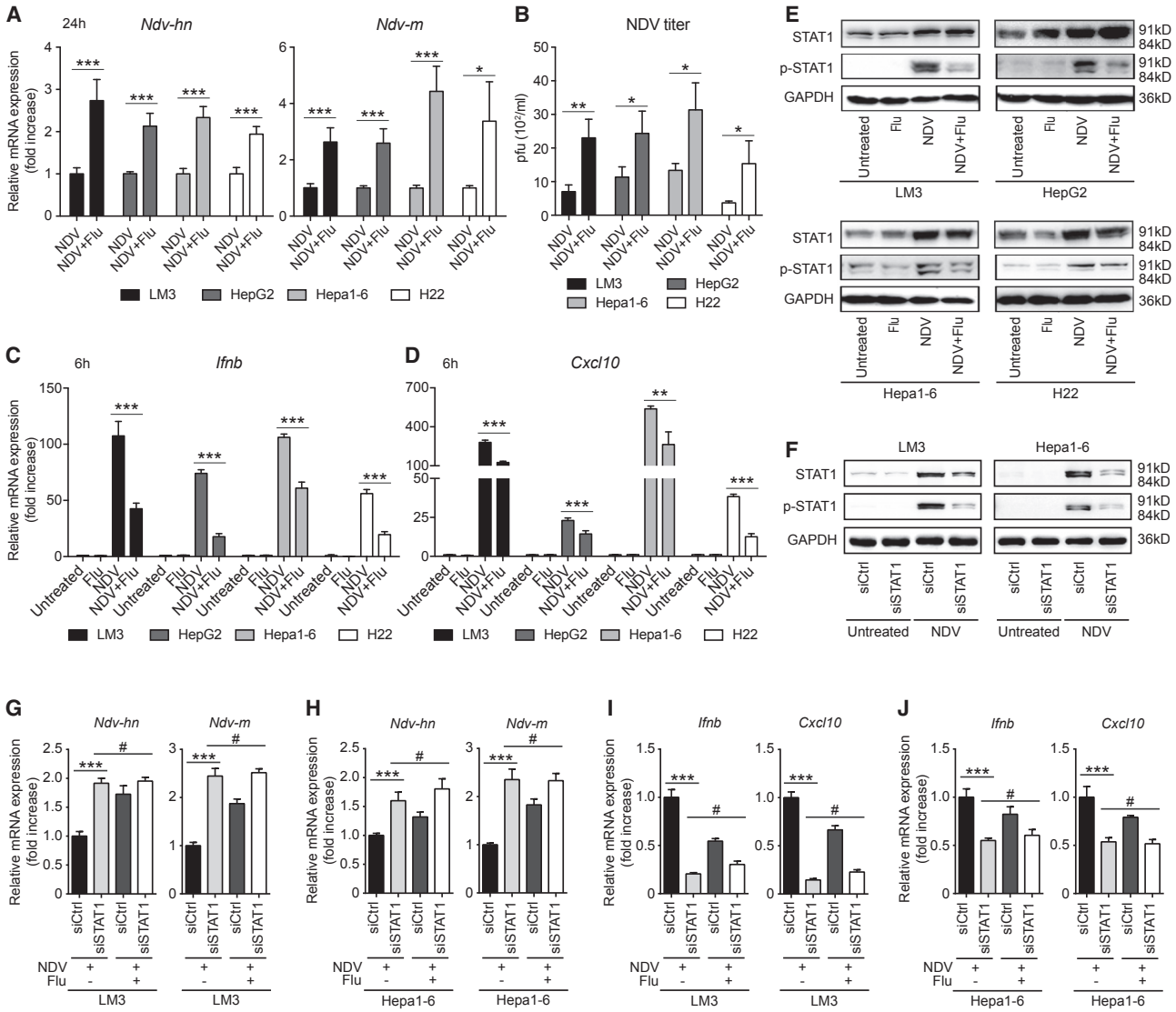

Figure 2. Fludarabine Promotes NDV Replication by Inhibiting STAT1 Activation in HCC Cells

(A–D) LM3, HepG2, Hepa1-6, and H22 cells were infected with NDV (MOI = 10) in the presence or absence of fludarabine (200 nM) (A and B) for 24 h and harvested, *Ndv-hn* and *Ndv-m* expression was determined by qPCR (A), and NDV titers were measured by plaque assay (B); or (C and D) for 6 h and harvested, and *Ifnb* (C) and *Cxcl10* (D) expression was determined by qPCR. qPCR results are means + SDs of quadruplicates, NDV titers are means + SD of triplicates. (E) Cells were infected with NDV (MOI = 10) for 12 h in the presence or absence of fludarabine (200 nM) and lysed, and the total STAT1 and phosphorylated STAT1 levels were determined by western blotting. (F–J) LM3 and Hepa1-6 cells were transfected with an siRNA targeting STAT1 (siSTAT1) for 24 h, infected with NDV (MOI = 10) for 6 h (F, I, and J) or 24 h (G and H) in the presence or absence of fludarabine (200 nM) and lysed, and (F) the total STAT1 and phosphorylated STAT1 (p-STAT1) levels were determined by western blotting. (G and H) *Ndv-hn* and *Ndv-m* expression in LM3 cells (G) and Hepa1–6 cells (H). (I and J) *Ifnb* and *Cxcl10* expression in LM3 (I) and Hepa1–6 (J). Cells were quantified by qPCR. A non-specific siRNA (siCtrl) was used as a control. Means + SDs of quadruplicates are shown. *p < 0.05; **p < 0.01; ***p < 0.001; #not significant.

(hemagglutinin-neuraminidase) and *Ndv-m* (matrix) genes. Fludarabine (200 nM) increased NDV replication 2- to 6-fold in HCC cells at 24 h after infection (Figures 2A and 2B). We then evaluated the expression of *Ifnb* (IFN-β) and *Cxcl10* (C-X-C motif chemokine 10), key cellular innate antiviral factors. Viral infection was unaffected by fludarabine (Figure S2), however, *Ifnb* and *Cxcl10* expression were significantly reduced by fludarabine at 6 h after infection (Figures 2C and 2D), suggesting that fludarabine may promote viral replication by mitigating antiviral innate immunity.

To further clarify how fludarabine downregulated *Ifnb* and *Cxcl10* expression in cells, we assessed the activation of STAT1. In

HCC cells, STAT1 was activated by NDV at 12 and 24 h after infection (Figure S3), and it was significantly reduced by fludarabine (Figure 2E). We further found that STAT1 silencing by siRNA (Figure 2F) increased viral replication in HCC cells similarly to fludarabine. Moreover, fludarabine failed to increase viral replication in STAT1-silenced HCC cells (Figures 2G and 2H). Consistently, both STAT1 silencing and fludarabine reduced *Ifnb* and *Cxcl10* expression in NDV-infected HCC cells, and fludarabine did not suppress innate antiviral immunity in STAT1-silenced cells (Figures 2I and 2J). Taken together, fludarabine increases NDV replication in HCC cells by inhibiting the activation of STAT1.

Fludarabine Mitigates NDV-Induced Activation of STAT3 by Accelerating Ubiquitin-Proteasomal Degradation

STAT3 participates in cancer-related inflammation, cellular transformation, and immune suppression. NDV infection activated STAT3 (phosphorylated STAT3, p-STAT3) at 12, 24, and 48 h after infection (Figure 3A). Interestingly, NDV-induced STAT3 activation was markedly reduced by fludarabine (Figure 3B). In addition, the expression of *Il-6*, a pro-tumor inflammatory cytokine and downstream target of STAT3, was markedly upregulated by NDV but was reduced by fludarabine to ca. 50% to 70% (Figure 3C). These results suggest that fludarabine ameliorates NDV-induced inflammation by targeting STAT3 signaling in HCC cells. Next, we evaluated the mechanism by which fludarabine promotes degradation of p-STAT3. First, we investigated the role of STAT1. In STAT1-silenced HCC cells, the p-STAT3 level was not reduced by viral infection, and the fludarabine-induced decrease in p-STAT3 level was not recovered (Figure 3D). These data suggest that STAT1 signaling is not involved in the fludarabine-mediated inhibition of p-STAT3 in HCC cells. Second, we evaluated the role of autophagy in fludarabine-induced p-STAT3 degradation. At 2, 6, 12, and 24 h, we determined the ratio of microtubule-associated proteins 1A/1B light chain 3B (LC3-II/I). However, fludarabine did not increase the LC3-II/I ratio (a marker of autophagosome formation) in HCC cells (Figure 3G, lower), which indicates that p-STAT3 is not degraded in the autophagosome. However, in NDV infected HCC cells, the fludarabine induced reduction in p-STAT3 level was almost completely blocked by the proteasome inhibitor MG132 (Figure 3E), which indicates that proteasomal degradation is involved in the elimination of p-STAT3. Moreover, cellular proteasomal activity was not altered by fludarabine in infected or uninfected HCC cells (Figure 3F). However, the levels of polyubiquitinated proteins, particularly those of similar size to p-STAT3 (75–100 kDa; Figure 3G) were affected by fludarabine. Following fludarabine treatment, the levels of polyubiquitinated proteins increased at 2 and 6 h and decreased at 12 and 24 h; the p-STAT3 level was also decreased at the latter two time points (Figure 3G, left). Therefore, fludarabine induces ubiquitin-proteasomal degradation of p-STAT3.

Fludarabine Antagonizes NDV-Induced IDO1 by Promoting Proteasomal Degradation

IDO1 plays a crucial role in tumor-associated immunosuppression and is upregulated during an immune response. IDO1 protein and mRNA levels were significantly increased in NDV-infected HCC cells (Figures 4A and 4B). Fludarabine dramatically decreased the NDV-induced increase in IDO1 level (Figure 4C). Interestingly, fludarabine significantly increased *Ido1* mRNA expression in NDV-infected LM3 and Hepa1-6 HCC cells (Figure 4D). Moreover, in HCC cells treated with fludarabine and MG132, IDO1 expression was almost completely recovered (Figure 4E). Therefore, fludarabine promotes proteasomal degradation of IDO1 in NDV-infected HCC cells.

Fludarabine Increases NDV Replication *In Vivo* and Enhances NDV-Mediated Antitumor Immunity

In a mouse model of ascitic HCC (Figure 5A), fludarabine increased NDV replication 2- to 13-fold in ascitic cells on days 12 and 16 after tumor transplantation (Figures 5B and 5C) and markedly promoted p-STAT3 and IDO1 degradation (Figures 5D). Moreover, NDV induced an overall immune response in ascites, which was significantly increased by fludarabine (Figure 5E). Consistently, *Ifnb, Cxcl10,* and *Ifnb* expression was significantly upregulated by NDV and further increased by fludarabine (Figure 5F). Moreover, $CD8^+$ T and $NK1.1^+$ cell infiltration in ascites was increased almost 2-fold by NDV (Figures 5G and 5H). Interestingly, infiltration of NK cells, but not $CD8^+$ T cells, was further significantly increased by fludarabine (Figures 5G and 5H). Notably, fludarabine at 7.5 mg/mouse did not have significant cytotoxic effects on $CD8^+$ T and NK cells (Figures 5G and 5H). Surprisingly, NDV increased the number of MDSCs in ascites ($CD11b^+Gr\text{-}1^{int}$); importantly, fludarabine antagonized this effect (Figure 5I). Thus, fludarabine increases the oncolytic effects of NDV by upregulating viral replication, promoting degradation of p-STAT3 and IDO1, increasing NK cell infiltration, and reducing the number of MDSCs.

Fludarabine Enhances the Antitumor Efficacy of NDV

Next, we investigated the antitumor efficacy of NDV plus fludarabine *in vivo*. In the ascitic HCC model (Figure 6A), fludarabine enhanced the antitumor efficacy of NDV (Figures 6B and S5B) resulting in prolonged survival (Figure 6C). Of note, the abdomen circumference was markedly reduced in two of seven mice (Figure S5A), and one mouse acquired a complete response to the combination treatment (Figure 6C). In a subcutaneous HCC model (Figure 6D), fludarabine significantly enhanced the therapeutic efficacy of NDV (Figure 6E) and prolonged the survival. Three out of seven mice obtained completed responses to the combination treatment (Figure 6F). No obvious therapy-associated side effect or body-weight loss was recorded (Figures S5C and S5D). These results indicate that fludarabine improves the antitumor efficacy of NDV.

Fludarabine Antagonizes IFN-γ-Induced STAT3 Activation and Upregulation of IDO1

Negative feedback plays a crucial role in immune homeostasis and cancer-associated immune suppression. We further determined the influence of fludarabine on p-STAT3 and IDO1 in the presence of IFN-γ, which was upregulated by NDV (Figure 5E). While STAT3 was activated by IFN-γ at 2 and 12 h (Figure 7A), it was massively reduced by fludarabine (Figure 7B). Furthermore, MG132 abrogated the fludarabine-mediated reduction in p-STAT3 level, which

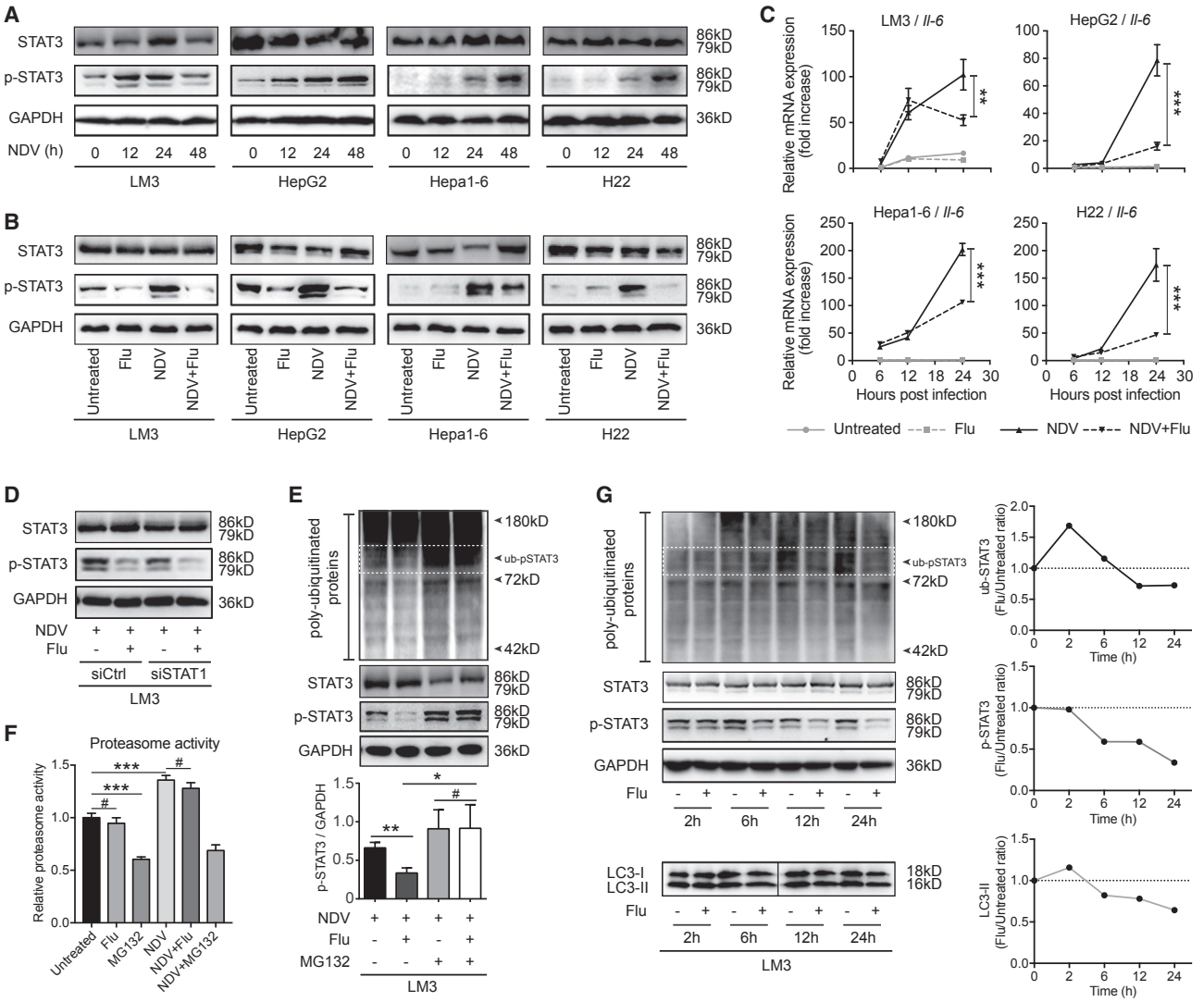

Figure 3. Fludarabine Induces Ubiquitin-Proteasomal Degradation of Activated STAT3

(A) LM3, HepG2, Hepa1-6, and H22 cells were infected with NDV (MOI = 10) for 0, 12, 24, or 48 h and lysed, and the STAT3 and phosphorylated STAT3 (p-STAT3) levels were determined by western blotting. (B) Cells were infected with NDV (MOI = 10) for 24 h in the presence or absence of fludarabine (200 nM) and lysed, and the STAT3 and p-STAT3 levels were determined by western blotting. (C) Cells were infected with NDV (MOI = 10) for 6, 12, or 24 h in the presence or absence of fludarabine (200 nM) and harvested, and *Il-6* expression was determined by qPCR. Means + SDs of quadruplicates are shown. (D) LM3 cells were transfected with an siRNA targeting STAT1 (siSTAT1) or a non-specific control siRNA (siCtrl) for 24 h, infected with NDV (MOI = 10) in the presence or absence of fludarabine (200 nM) and lysed, and the STAT3 and p-STAT3 levels were determined by western blotting. (E) LM3 cells were infected with NDV (MOI of 10) for 24 h in the presence or absence of fludarabine (200 nM) or MG132 (10 μM, proteasome inhibitor) and lysed, and the p-STAT3 and polyubiquitinated protein levels were determined by western blotting. Representative blots (left) and p-STAT3/GAPDH intensity ratios from three independent experiments (right) are shown. (F) LM3 cells were infected with NDV (MOI = 10) for 12 h in the presence or absence of fludarabine (200 nM), and the cellular proteasomal activity was measured. Means + SDs of quadruplicates are shown. (G) LM3 cells were treated with fludarabine (200 nM) for 2, 6, 12, or 24 h and lysed, and the polyubiquitinated protein, STAT3, p-STAT3, and LC3-I/II levels were determined by western blotting. GAPDH was used as a loading control. *p < 0.05; **p < 0.01; ***p < 0.001; #not significant.

indicates promotion of its proteasomal degradation in the presence of IFN-γ. Similarly, IFN-γ-mediated upregulation of IDO1 was blocked by fludarabine (Figure 7C). The results indicate that fludarabine counters IFN-γ-induced immune-negative feedback such as activation of STAT3 and upregulation of IDO1.

DISCUSSION

OV-mediated viro-immunotherapy for cancer shows much promise; however, its clinical use is hampered by limited viral replication and immune-negative feedback. Here, we report that fludarabine is an effective adjuvant for oncolytic viro-immunotherapy. Fludarabine

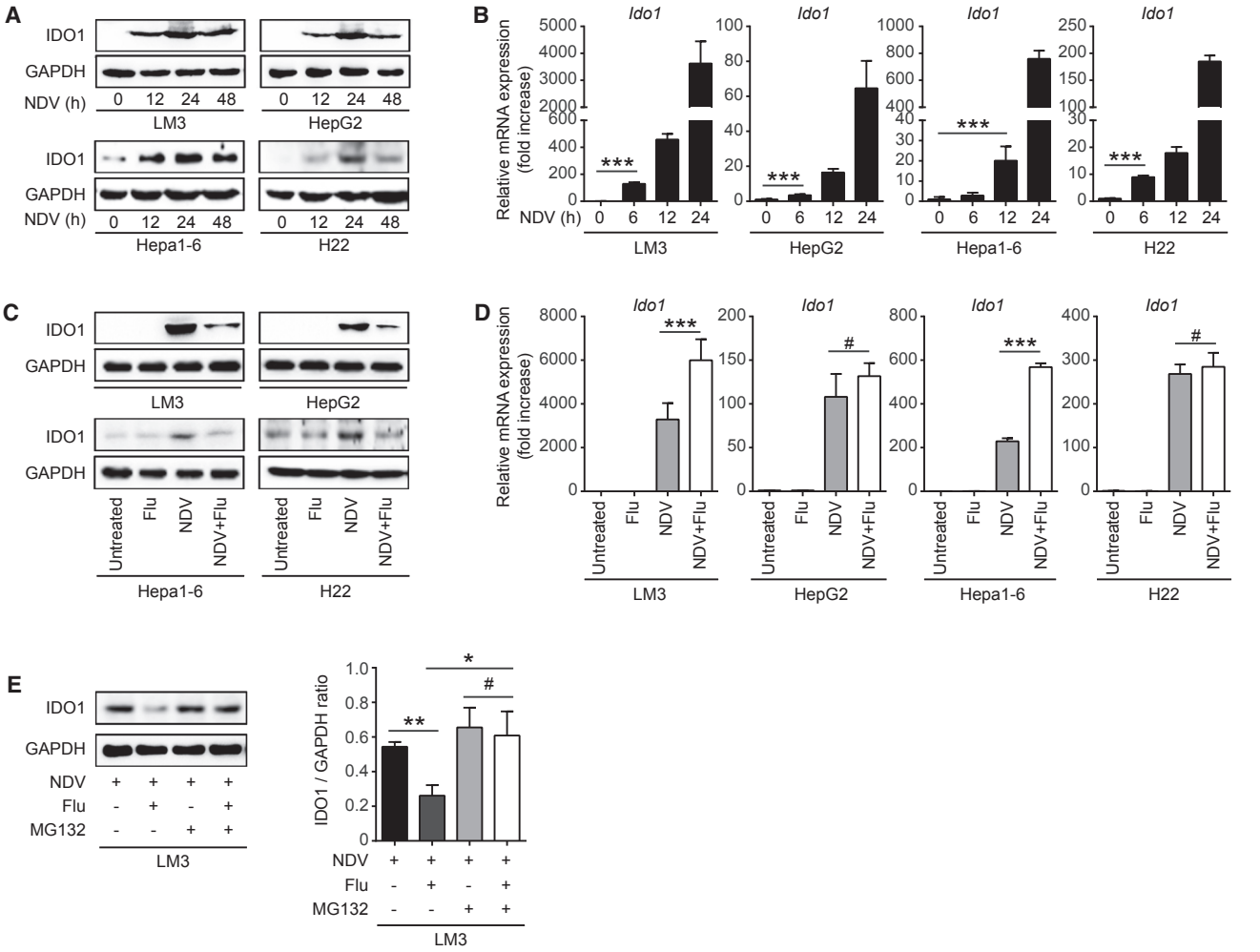

Figure 4. Fludarabine Accelerates the Proteasomal Degradation of IDO1

(A and B) LM3, HepG2, Hepa1-6, and H22 cells were infected with NDV (MOI = 10) for 0, 6, 12, 24, or 48 h, harvested, and the IDO1 (A) protein level was quantified by western blotting and (B) mRNA level by qPCR. (C and D) Cells were infected with NDV (MOI = 10) in the presence or absence of fludarabine (200 nM) for 24 h and lysed, and the IDO1 (C) protein level was determined by western blotting and (D) the mRNA level by qPCR. Means + SDs of quadruplicates are shown. (E) LM3 cells were infected with NDV (MOI = 10) in the presence or absence of fludarabine (200 nM) or MG132 (10 μM) for 24 h, and the IDO1 protein level was determined by western blotting. Representative blots (left) and IDO1/GAPDH intensity ratios of three independent experiments (right) are shown. GAPDH was used as a loading control. *$p < 0.05$; **$p < 0.01$; ***$p < 0.001$; #not significant.

enhanced NDV-mediated viro-immunotherapy by promoting viral replication by targeting STAT1, which enhanced oncolysis, and promoting NDV-induced antitumor immune responses by accelerating the ubiquitin-proteasomal degradation of p-STAT3 and IDO1, increasing NK cell infiltration and reducing the number of MDSCs in the TME (Figure 8). Thus, fludarabine and NDV represent a promising oncolytic viro-immunotherapy.

Efficient replication in cancer cells is a crucial determinant for oncolytic virotherapy. Viral replication is mainly dependent on cell viability and host cellular antiviral innate immunity. Replication of oncolytic measles virus in lymphoma cells was increased by fludarabine; however, the mechanism is unknown.[36] In this study, fludarabine at a low dose had little impact on cell viability but significantly enhanced NDV replication. We previously reported that autophagic flux favored oncolytic NDV replication by preventing virus-induced apoptosis.[37] Fludarabine did not induce *de novo* formation of autophagosomes. Type I IFNs induce STAT1 expression as a part of positive feedback loop to augment the extent and duration of IFN responses,[38–41] which may limit viral replication.[15,42] Thus, as an inhibitor of STAT1,[33] fludarabine promoted NDV replication by suppressing the production of type I IFNs at the early stage (Figure 2C). However, when more viral yields were generated, the production of type I IFNs was increased accordingly (Figures 5F and S4), which may further participate in immune activation.

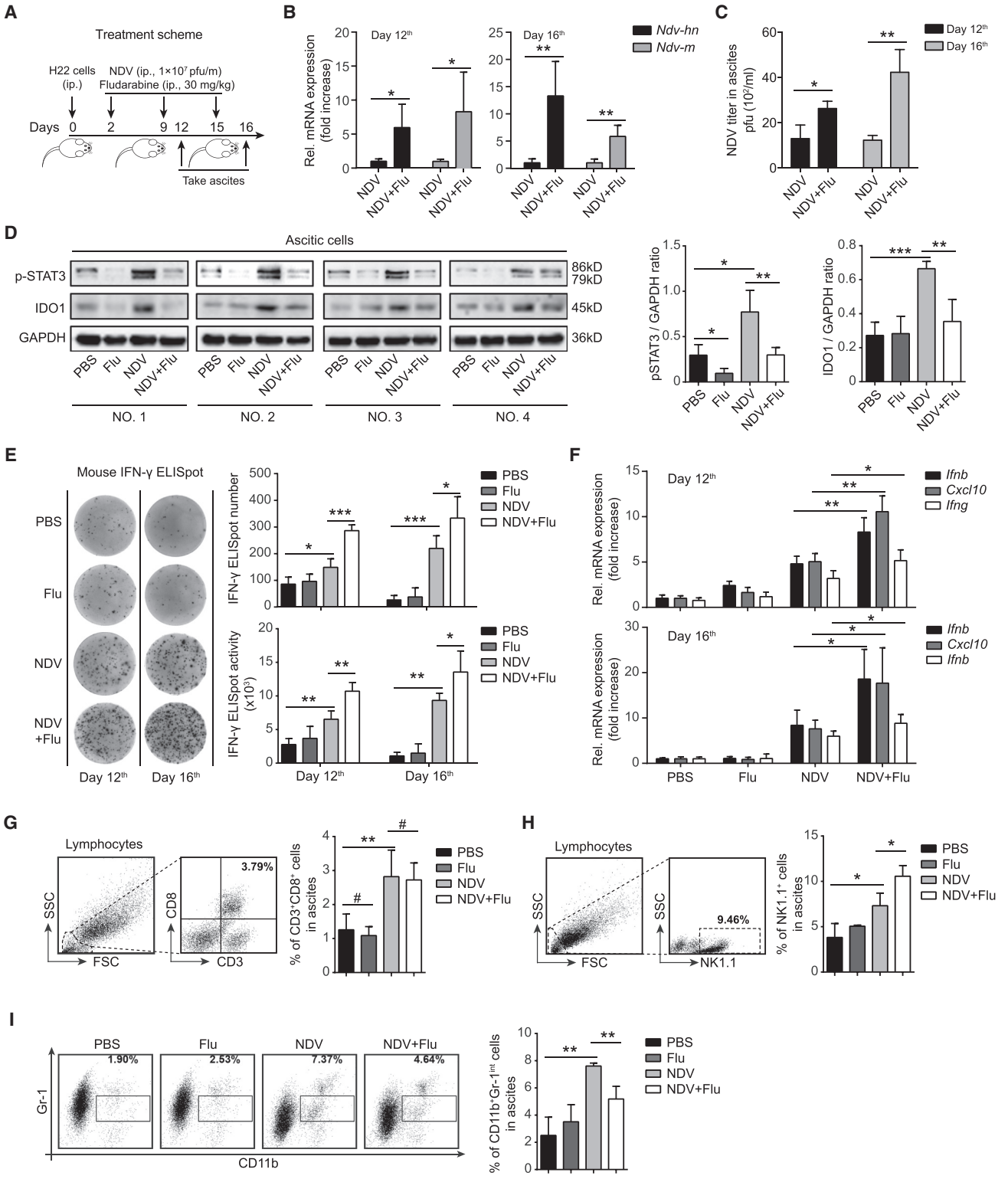

Figure 5. Fludarabine Enhances NDV-Induced Antitumor Immunity *In Vivo*

(A) Mice received an ip. injection of 2×10^6 H22 cells followed by 1×10^7 pfu NDV with or without fludarabine (30 mg/kg, ip.) at the indicated time points (n = 4 per group). (B and C) Ascitic cells were harvested at days 12 and 16, *Ndv-hn* and *Ndv-m* expression was quantified by qPCR (B), and NDV titers were measured by plaque assay (C).

(legend continued on next page)

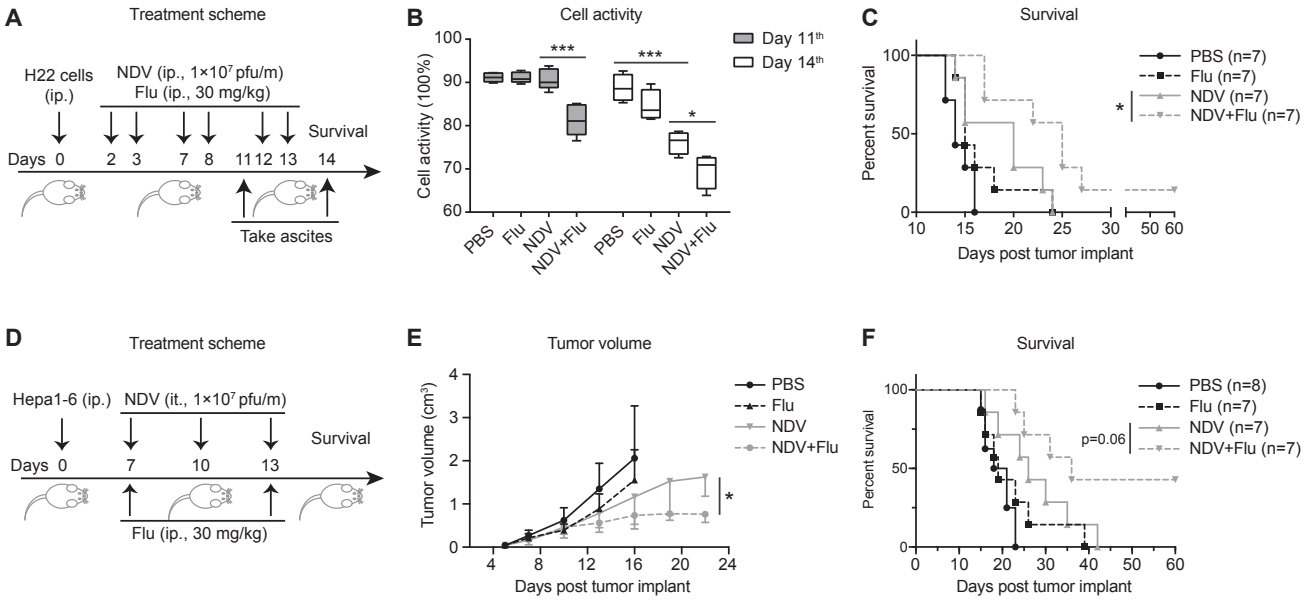

Figure 6. NDV and Fludarabine Achieve Superior Antitumor Outcomes *In Vivo*

(A) Mice received an ip. injection of 2×10^6 H22 cells. Two days later, mice were injected ip. with 1×10^7 pfu NDV with or without fludarabine (30 mg/kg, ip.) for six rounds at the indicated time points. Control mice received an equal dose of fludarabine (ip.) or equal volume of PBS (ip.) (n = 7 per group). (B) Ascitic cells were harvested and their viability determined by trypan-blue exclusion assay. (C) Survival was determined and plotted for Kaplan-Meier survival analysis and analyzed by log rank (Mantel-Cox) test. (D) Mice were injected subcutaneously with 5×10^6 Hepa1-6 cells. On days 7, 10, and 13, the mice received intratumoral injection of 1×10^7 pfu NDV, combined with intraperitoneal injection of fludarabine (0.75 mg/mouse, gray dashed line) on day 7 and day 13, respectively. Mice that received equal doses of NDV or fludarabine or PBS alone were used as controls. (E) Tumor volumes were measured by caliper every 2–3 days before treatment. Means + SDs of each group are shown. (F) Survival was analyzed by log rank (Mantel-Cox) test. *$p < 0.05$; ***$p < 0.001$.

Activated STAT3 and IDO1 participate in cancer-associated immunosuppression,[21,26,43] and their expression in cancer cells is induced by immune stimulation such as viral infection, IFNs, and adoptive immune cell therapy.[34] Elevated levels of p-STAT3 and IDO1 are detrimental to viro-immunotherapy. Fludarabine is suitable for oncolytic viro-immunotherapy, as it suppressed NDV-activated IL-6/STAT3 signaling and IDO1 upregulation. Moreover, fludarabine significantly reduced p-STAT3 and IDO1 expression in HCC cells treated with IFN-γ, the level of which is markedly elevated during an antitumor immune response. Activated STAT3 is mainly degraded via the ubiquitin-proteasome pathway.[44–47] In line, we found that fludarabine promoted proteasomal degradation of p-STAT3 in HCC cells, not by increased activity of proteasome but by enhanced ubiquitination of the target protein. Similarly, fludarabine accelerated the NDV- or IFN-γ-induced ubiquitin-proteasomal degradation of IDO1 in HCC cells. A previous study showed that IDO1 participated in IFN-γ-mediated antiviral effect,[48] it would be interesting to know if NDV replication might also benefit from enhanced degradation of IDO1 by fludarabine observed *in vivo*.

NDV elicits both an innate and adaptive immune response in the TME by inducing IFN production and immune cell infiltration and maturation.[7–9,11,12] In this study, local injection of NDV in HCC induced an immune response and infiltration of $CD8^+$ T and NK cells in the TME. Indeed, fludarabine enhanced overall immune response induced by NDV in the ascitic fluid. Direct activation of NK cells contributes to the antitumor effects of NDV.[49] NDV-induced NK-cell infiltration was further increased by fludarabine, possibly by increasing NDV replication.

Immunosuppressive MDSCs comprise granulocytic $CD11b^+Gr\text{-}1^{high}$ cells and monocytic $CD11b^+Gr\text{-}1^{int}$ cells, the latter subset of which is most suppressive. NDV infection induced polarization of monocytes to $CD11b^+Gr\text{-}1^{int}$ MDSCs, which may repress antitumor immunity. Surprisingly, fludarabine significantly decreased the number of MDSCs in the TME. Because the differentiation of MDSCs depends on STAT3 activation,[18] this decrease in the number of MDSCs was likely due to accelerated degradation of p-STAT3. Furthermore, as IDO1 is correlated with the expansion, recruitment, and activation

(D) Ascitic cells were harvested at day 16, and IDO1 and phosphorylated STAT3 protein levels (left) and IDO1/GAPDH and p-STAT3/GAPDH intensity ratios (right) were evaluated. (E) Ascitic cells were harvested on days 12 and 16, washed, counted, and subjected to the IFN-γ ELISpot assay. (F) Ascitic cells were harvested on days 12 and 16, and *Ifnb, Cxcl10,* and *Ifng* expression was quantified by qPCR. (G–I) Ascitic cells were harvested on day 16 and subjected to flow cytometry analyses of (G) $CD3^+CD8^+$ cells, (H) $NK1.1^+$ cells, and (I) $CD11b^+Gr\text{-}1^{int}$ cells. *$p < 0.05$; **$p < 0.01$; ***$p < 0.001$; #not significant.

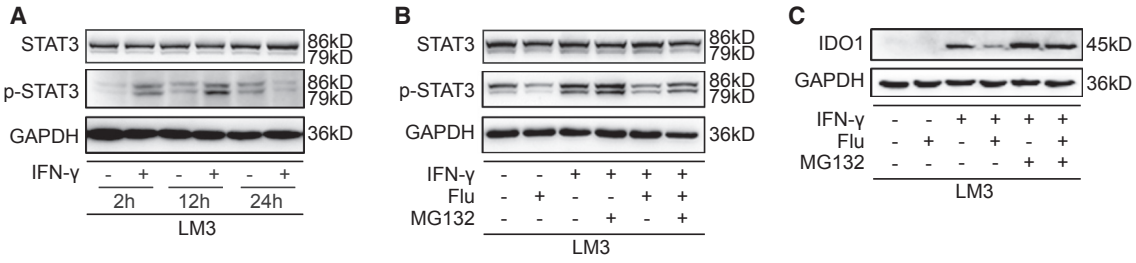

Figure 7. Fludarabine Antagonizes IFN-γ-Induced STAT3 Activation and Upregulation of IDO1 in HCC Cells

(A) LM3 cells were treated with IFN-γ (2,000 IU/mL) for 2, 12, or 24 h, lysed, and STAT3/p-STAT3 protein levels were determined by western blotting. (B and C) LM3 cells were treated with fludarabine (200 nM) and IFN-γ (2,000 IU/mL) for 12 (B) or 24 (C) h in the presence of MG132 (10 μM) and lysed, and STAT3 activation (B) and IDO1 expression (C) were assayed by western blotting. GAPDH was used as a loading control. Representative blots of two independent experiments are shown.

of MDSCs in tumors,[50] the fludarabine-induced decrease in IDO1 expression might also have led to a reduction in the number of MDSCs. The ascitic HCC tumor model used in this study facilitates dynamic monitoring of viral replication, oncolysis, immune activation, and cell infiltration. Finally, the antitumor potency of fludarabine with NDV was validated in a subcutaneous HCC tumor model.

In conclusion, NDV induced an antitumor immune response in the TME as well as negative feedback, such as STAT3 activation, and increased IDO1 and MDSCs. Fludarabine not only promotes viral replication by targeting STAT1 but also accelerates proteasomal degradation of p-STAT3 and IDO1 and reduces the number of infiltrating MDSCs. These effects of fludarabine significantly prolong the survival of HCC-bearing mice. Our findings suggest the potential of fludarabine as an adjuvant for oncolytic viro-immunotherapy, but further work is required before it can be used clinically.

MATERIALS AND METHODS

Cell Culture and Reagents

The human HCC cell line HCCLM3 and mouse HCC cell line H22 were obtained from the China Center for Type Culture Collection; the human HCC cell line HepG2 and mouse HCC cell line Hepa1-6 were obtained from the Cell Bank of Type Culture Collection Chinese Academy of Sciences. These cell lines were authenticated by short tandem repeat (STR) analysis and tested for mycoplasma contamination. HCCLM3 (abbreviated LM3), HepG2, and Hepa1-6 cells were cultured in DMEM, whereas H22 cells were cultured in RPMI 1640, supplemented with 10% fetal bovine serum (FBS), 2 mM L-glutamine, 100 units/mL penicillin, and 0.1 mg/mL streptomycin (all from Thermo Fisher Scientific, Gibco, Grand Island, NY, USA), and maintained in a humidified incubator with atmosphere containing 5% CO_2 at 37°C.

The following reagents were used in this study: fludarabine monophosphate (#F0913; Tokyo Chemical Industry, Tokyo, Japan), MG132 (#M8699; Sigma-Aldrich, St. Louis, MO, USA), human IFN-γ (#Z02915; GenScript, Piscataway, NJ, USA), trypan blue (#ST798; Beyotime Biotechnology, Shanghai, China), and 3-(4,5-dimethyl-2-thiazolyl)-2,5-diphenyl-2H-tetrazolium bromide (MTT) (#M2128; Sigma-Aldrich).

NDV Propagation, Viral Titers, and Infection

The NDV La Sota strain was a gift from Prof. Y. Wang (Jiangsu Academy of Agricultural Sciences, China), propagated in 9-day-old specific-pathogen-free (SPF) embryonated chicken eggs from seed virus, harvested from the allantoic fluid, and purified by centrifugation at 3,000 rpm for 10 min. The viral particles in the supernatant were harvested and cryopreserved at −80°C. Viral titers were determined by plaque assay. In brief, samples were serially diluted, and 100 μL of each dilution was added per well to Vero cells in 12-well plates. 2 h later, DMEM (containing 2 μg/mL N-tosyl-L-phenylalanine chloromethyl ketone [TPCK]-treated trypsin, 2% FBS, and 0.8% agar) was added and cells were incubated at 37°C for 4 days. Then cells were fixed with 4% paraformaldehyde solution and stained with 0.5% neutral red solution for observation of plaques.

Tumor cells were washed once with PBS and infected with NDV in OptiMEM (Thermo Fisher Scientific, Gibco) at the indicated MOI for 2 h, and complete medium was added to each well.

Cytotoxic Effect Assay

MTT Cell Viability Assay

Cells were seeded in 96-well plates and treated with fludarabine, NDV, or both at the indicated doses. Cell viability was determined after 48 h of incubation by adding 100 μL MTT solution (1 mg/mL). Following 4 h incubation at 37°C, the MTT solution was aspirated and 150 μL isopropanol were added to solubilize formazan, followed by shaking for 15 min. The absorbance at 570 nm was recorded using the SpectraMax M3 Multi-Mode Microplate Reader (Molecular Devices, Sunnyvale, CA, USA).

Trypan Blue Exclusion

Cells were harvested using trypsin-EDTA (0.25%) solution (Thermo Fisher Scientific, Gibco) and stained with trypan blue solution; viability was determined by trypan blue exclusion using the Countstar Automated Cell Counter (Inno-Alliance Biotech, Wilmington, DE, USA). The cell death (%) was calculated as number of dead cells/total number of cells × 100%. The cell activity (%) was calculated as number of live cells/total number of cells × 100%.

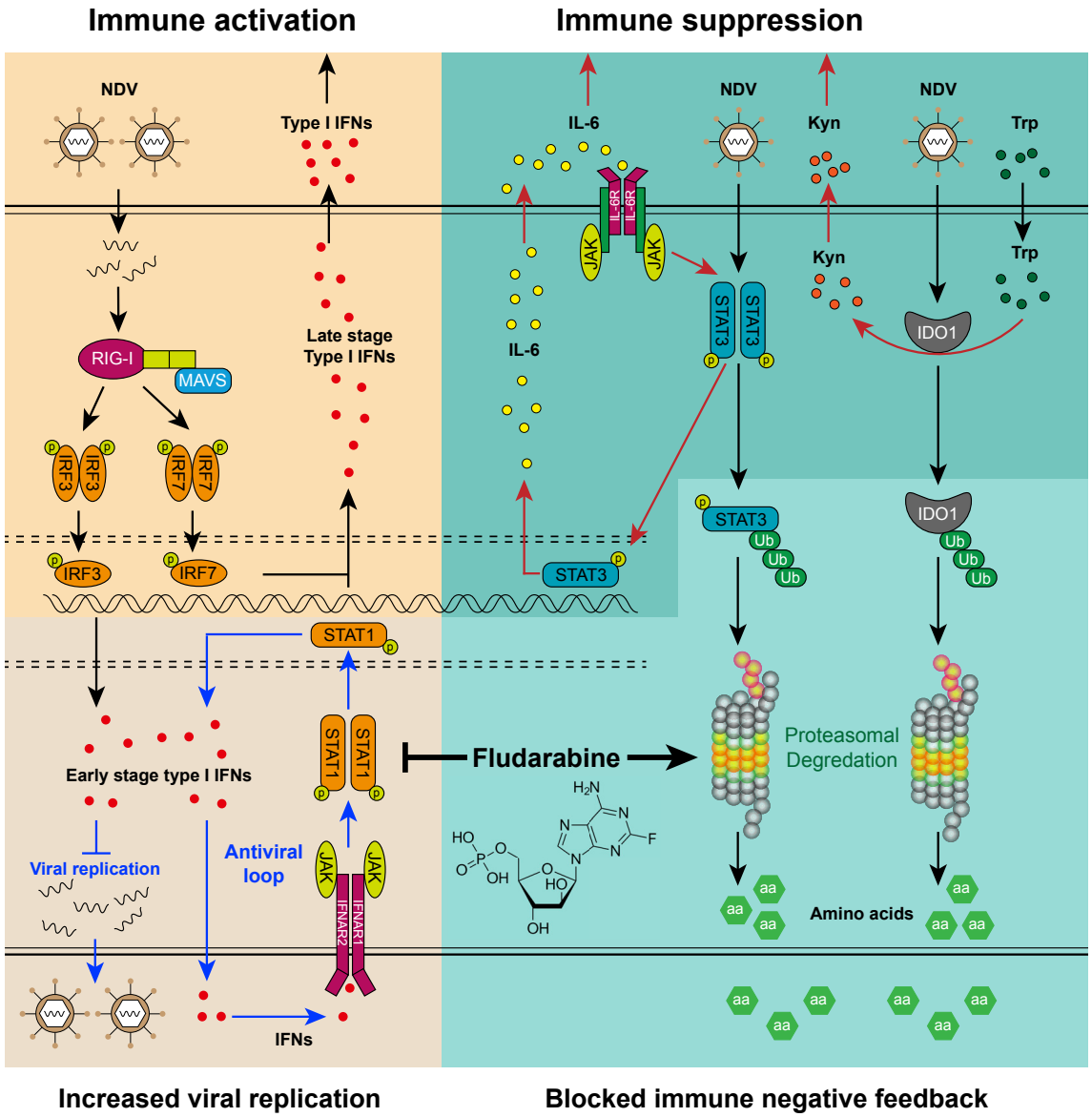

Figure 8. Fludarabine Improves NDV-Mediated Oncolytic Viro-immunotherapy

On the one hand, the viral RNA activates the cytoplasmic RIG-I signaling pathway in the host cells to produce type I IFNs or other antiviral molecules. Autocrine or paracrine of IFNs activate STAT1 signaling pathway to amplify the antiviral loop. Fludarabine blocks this feedforward loop and favors viral replication at an early stage after infection. Increased viral replication in the host cells results in more IFN production at the late stage of infection, which further activates antitumor immune responses (left). On the other hand, fludarabine increases proteasomal degradation of p-STAT3 and IDO1 by accelerating ubiquitination of target proteins, in turn, blocks immune suppression (right). Abbreviations: RIG-I, retinoic acid-inducible gene I; MAVS, mitochondrial antiviral-signaling protein; IRF3/7, interferon regulatory factor 3/7; IFNAR, interferon-α/β receptor; JAK, Janus kinase; IL-6R, interleukin-6 receptor; Ub, ubiquitin; Trp, tryptophan; Kyn, kynurenine.

Western Blot

Cells were lysed in RIPA buffer (#P0013C; Beyotime) containing protease inhibitor tablets (#05892791001; Roche, Indianapolis, IN, USA). Protein concentration was determined using an enhanced BCA protein assay kit (#P0010, Beyotime). Equal amounts of protein were separated by SDS-PAGE and electrophoretically transferred to a polyvinylidene fluoride membrane (#03010040001; Roche). After blocking in 5% nonfat milk in Tris-buffered saline, the membrane was incubated with specific primary antibodies, followed by appropriate horseradish peroxidase (HRP)-conjugated secondary antibodies. Signals were detected using an enhanced chemiluminescence reagent (#WBKLS0500, Millipore, Billerica, MA, USA) and subjected to chemiluminescent imaging system (ChampChemi 610, Sage Creation Science, Beijing, China). The following antibodies were

used: anti-GAPDH (#MB001; 1:5,000; Bioworld, St. Louis Park, MN, USA), anti-Stat1 (#A0027; 1:500; ABclonal, Wuhan, China), anti-phospho-Stat1(Tyr701) (58D6) (#9167; 1:1,000; Cell Signaling Technology, Danvers, MA, USA), anti-Stat3 (#9139; 1:1,000; Cell Signaling Technology), anti-phospho-Stat3(Tyr705) (D3A7) (#9145; 1:1,000; Cell Signaling Technology), anti-IDO1 (#ab55305 and ab106134; 1:500; Abcam, Cambridge, MA, USA), anti-ubiquitin (#10201-2-AP; 1:500; Proteintech, Rosemont, IL, USA), as well as HRP-conjugated secondary antibodies (#31430 and 31460; 1:2,000; Thermo Fisher Scientific, Pierce).

Quantitative RT-PCR

Total cellular RNA was extracted with TRIzol (#15596-026; Thermo Fisher Scientific, Invitrogen) and was reverse-transcribed using PrimeScript™ RT Master Mix (#DRR036A, TaKaRa, Shiga, Japan). Quantitative PCR was performed using FastStart Universal SYBR Green Master Mix (#04913914001; Roche) on a ViiA 7 Real-Time PCR System (Applied Biosystems, Foster, CA, USA). Gene expression was calculated by the comparative Ct method and normalized to that of GAPDH. Primer sequences are listed in Table S1.

Short Interfering RNA Transfection

Short interfering RNA (siRNA) (100 nM) coupled with Lipofectamine™ 2000 (#11668019; Thermo Fisher Scientific, Invitrogen) was used for transfection on a 6- or 12-well plate according to the manufacturer's instructions. The sequences of siRNA targeting STAT1 and non-specific control siRNA are listed in Table S1. NDV infection or drug treatment was performed at 24 h after siRNA transfection in STAT1-silencing experiments.

Animal Experiments and Tumor Models

Six-week-old male C57BL/6 mice were obtained from the Model Animal Research Center of Nanjing University (Nanjing, China). Experiments were conducted according to the ethical guidelines approved by the local government.

The Ascitic HCC Tumor Model

For immune-activation experiments, tumors were implanted by intraperitoneal (ip.) injection of 2×10^6 H22 cells on day 0. H22-bearing mice were randomized to four groups on day 2. On days 2, 9, and 15, the mice received an ip. injection of 1×10^7 plaque-forming units (pfu) of NDV per mouse in PBS in a total volume of 100 μL, followed 1 h later by ip. injection of 0.75 mg/mouse fludarabine monophosphate solution in a total volume of 100 μL. The control groups received an equal volume of PBS intraperitoneally. On days 12 and 16, ascites samples (500 μL) were removed for determination of NDV replication, antiviral gene expression, immune cell infiltration, IFN-γ enzyme-linked immune absorbent spots (ELISpots), IDO1 expression, and STAT3 phosphorylation. For oncolysis and survival experiments, tumors were implanted by ip. injection of 5×10^6 H22 cells on day 0. H22-bearing mice were randomized to four groups on day 2. On days 2, 3, 7, 8, 12, and 13, the mice received an ip. injection of 1×10^7 pfu of NDV per mouse in PBS in a total volume of 100 μL, followed 1 h later by an ip. injection of 0.75 mg/mouse fludarabine monophosphate solution in a total volume of 100 μL. The control groups received an equal volume of PBS intraperitoneally. On days 12 and 16, ascites samples (100 μL) were removed for determination of cell number and activity. The body weight and behaviors of the mice were monitored every other day, and their survival was monitored daily.

The Subcutaneous HCC Tumor Model

6- to 8-week-old male C57/BL6 mice received subcutaneous injection of 5×10^6 Hepa1-6 cells of each. On days 7, 10, and 13, the mice received intratumoral (it.) injection of 1×10^7 pfu NDV per mouse, respectively. On days 7 and 13, the mice received intraperitoneal injection of 0.75 mg/mouse fludarabine monophosphate solution in a total volume of 100 μL. The mice received equal volume of PBS were used as untreated control. Tumor volume was monitored every 2–3 days by caliper measurement and calculated by length × width × width/2.

Flow Cytometry

For immune activation experiments *in vivo*, ascitic cells were harvested and washed twice with PBS and incubated with the following antibodies: anti-NK1.1 (clone PK136, #553164), CD11b (clone M1/70, #557396), Gr-1 (clone RB6-8C5, #553128) (all from BD Biosciences, Franklin Lakes, NJ, USA); and anti-CD3e (clone 17A2, #17-00032-82), anti-CD8a (clone 53-6.7, #45-0081-82), and isotype antibodies (#45-4321-80, 11-4714-41, 17-4031-81, and 12-4321-81A) (all from Thermo Fisher Scientific, eBioscience). $CD11b^+$ $Gr\text{-}1^{int}$ cells were defined as MDSCs, and $CD3^+CD8^+$ cells were defined as $CD8^+$ T cells (cytotoxic T lymphocytes). Samples were subjected to flow cytometry using a FACS Calibur instrument (BD Biosciences), and data were analyzed using FlowJo software (v. 7.6.5, Tree Star, Ashland, OR, USA).

Proteasome Activity Assay

Proteasome activity was monitored based on the release of fluorescent 7-amido-4-methylcoumarin (AMC) from its tagged peptide substrate using a proteasome activity fluorometric assay kit (#K245-100; BioVision, Milpitas, CA, USA) according to the manufacturer's instructions. In brief, following treatment, cells were lysed with 0.5% NP-40. AMC standards, positive controls, and samples diluted in assay buffer were loaded in duplicate into a 96-well plate. The fluorescence activity was measured using the SpectraMax M3 Multi-Mode Microplate Reader at 37°C for 60 min at excitation and emission wavelengths of 350 and 445 nm, respectively. Proteasome activity was determined based on the standard curve.

IFN-γ Enzyme-Linked Immunosorbent Spot Assay

The activation status of immune cells in ascites was evaluated by the mouse IFN-γ EILSpot^{PLUS} kit (3321-2AW-Plus; Mabtech, Nacka Strand, Sweden) according to the manufacturer's protocols. In brief, ascites cells were seeded in a 96-well plate coated with an IFN-γ capture antibody at a density of 2×10^5 cells/well at 37°C for 24 h in a humidified incubator with an atmosphere containing 5% CO_2. The

cells were removed, the plate was washed five times with PBS, a biotinylated anti-IFN-γ antibody was added, and the plate was incubated at room temperature for 2 h. Next, the plate was washed with PBS, streptavidin-ALP was added, and the plate was incubated at room temperature for 1 h. Finally, the BCIP/NBT-plus substrate was added until spots emerged, and the plate was washed with tap water to stop the reaction. The plate was analyzed using an enzyme-linked immunosorbent spot (ELISpot) reader (Autoimmun Diagnostika, Strassberg, Germany) to enumerate spots, and spot activity was characterized as the weighted average of the spot size and intensity in a well.[30]

Statistical Analyses

Data were analyzed by the two-tailed unpaired Student's t test (for comparisons of two groups). Survival data were analyzed by the log rank (Mantel-Cox) test. Statistical analyses were conducted using Microsoft Excel (Microsoft, Redmond, WA, USA) or Prism software (v. 6.01; GraphPad).

SUPPLEMENTAL INFORMATION

Supplemental Information can be found online at https://doi.org/10.1016/j.omto.2019.03.004.

AUTHOR CONTRIBUTIONS

Conception and Design, J.W. and G.M.; Development of Methodology, G.M., B.L., C.X., and M.X.; Acquisition of Data (providing animals, acquiring and managing patients, providing facilities, etc.), G.M., Z.F., B.L., M.F., A.C., and D.Y.; Analysis and Interpretation of Data (e.g., statistical analysis, biostatistics, computational analysis), G.M., Z.F., and B.L.; Writing, Review, and/or Revision of the Manuscript, G.M. and J.W.; Administrative, Technical, or Material Support (i.e., reporting or organizing data, constructing databases), J.W., D.Y., and G.M.; Study Supervision, J.W.

CONFLICTS OF INTEREST

No potential conflicts of interest were disclosed.

ACKNOWLEDGMENTS

This work was supported by the National Natural Science Foundation of China (81773255, 81602702, 81472820, and 81871967), the Natural Science Foundation of Jiangsu Province of China (20160126), the Social Development Foundation of Jiangsu Province of China (BE2018604), the Project Funded by China Postdoctoral Science Foundation (2018M642223), Six Talent Peaks Project in Jiangsu Province to J.W., and Jiangsu Provincial Medical Talent to D.Y. The authors thank Prof. Y. Wang (Jiangsu Academy of Agricultural Sciences, China) for providing the NDV La Sota stain and Translational Medicine Core Facilities of Nanjing University for instrumental support.

REFERENCES

1. Pol, J., Kroemer, G., and Galluzzi, L. (2015). First oncolytic virus approved for melanoma immunotherapy. OncoImmunology *5*, e1115641.
2. Russell, S.J., Peng, K.W., and Bell, J.C. (2012). Oncolytic virotherapy. Nat. Biotechnol. *30*, 658–670.
3. Lichty, B.D., Breitbach, C.J., Stojdl, D.F., and Bell, J.C. (2014). Going viral with cancer immunotherapy. Nat. Rev. Cancer *14*, 559–567.
4. Workenhe, S.T., and Mossman, K.L. (2014). Oncolytic virotherapy and immunogenic cancer cell death: sharpening the sword for improved cancer treatment strategies. Mol. Ther. *22*, 251–256.
5. Kaufman, H.L., Kohlhapp, F.J., and Zloza, A. (2015). Oncolytic viruses: a new class of immunotherapy drugs. Nat. Rev. Drug Discov. *14*, 642–662.
6. Pol, J., Bloy, N., Obrist, F., Eggermont, A., Galon, J., Cremer, I., Erbs, P., Limacher, J.M., Preville, X., Zitvogel, L., et al. (2014). Trial Watch: Oncolytic viruses for cancer therapy. OncoImmunology *3*, e28694.
7. Zamarin, D., and Palese, P. (2012). Oncolytic Newcastle disease virus for cancer therapy: old challenges and new directions. Future Microbiol. *7*, 347–367.
8. Ginting, T.E., Suryatenggara, J., Christian, S., and Mathew, G. (2017). Proinflammatory response induced by Newcastle disease virus in tumor and normal cells. Oncolytic Virother. *6*, 21–30.
9. Lam, H.Y., Yeap, S.K., Pirozyan, M.R., Omar, A.R., Yusoff, K., Suraini, A.A., Abd-Aziz, S., and Alitheen, N.B. (2011). Safety and clinical usage of newcastle disease virus in cancer therapy. J. Biomed. Biotechnol. *2011*, 718710.
10. Elankumaran, S., Rockemann, D., and Samal, S.K. (2006). Newcastle disease virus exerts oncolysis by both intrinsic and extrinsic caspase-dependent pathways of cell death. J. Virol. *80*, 7522–7534.
11. Schwaiger, T., Knittler, M.R., Grund, C., Roemer-Oberdoerfer, A., Kapp, J.F., Lerch, M.M., Mettenleiter, T.C., Mayerle, J., and Blohm, U. (2017). Newcastle disease virus mediates pancreatic tumor rejection via NK cell activation and prevents cancer relapse by prompting adaptive immunity. Int. J. Cancer *141*, 2505–2516.
12. Koks, C.A., Garg, A.D., Ehrhardt, M., Riva, M., Vandenberk, L., Boon, L., De Vleeschouwer, S., Agostinis, P., Graf, N., and Van Gool, S.W. (2015). Newcastle disease virotherapy induces long-term survival and tumor-specific immune memory in orthotopic glioma through the induction of immunogenic cell death. Int. J. Cancer *136*, E313–E325.
13. Ricca, J.M., Oseledchyk, A., Walther, T., Liu, C., Mangarin, L., Merghoub, T., Wolchok, J.D., and Zamarin, D. (2018). Pre-existing Immunity to Oncolytic Virus Potentiates Its Immunotherapeutic Efficacy. Mol. Ther. *26*, 1008–1019.
14. Zamarin, D., Holmgaard, R.B., Subudhi, S.K., Park, J.S., Mansour, M., Palese, P., Merghoub, T., Wolchok, J.D., and Allison, J.P. (2014). Localized oncolytic virotherapy overcomes systemic tumor resistance to immune checkpoint blockade immunotherapy. Sci. Transl. Med. *6*, 226ra32.
15. Didcock, L., Young, D.F., Goodbourn, S., and Randall, R.E. (1999). The V protein of simian virus 5 inhibits interferon signalling by targeting STAT1 for proteasome-mediated degradation. J. Virol. *73*, 9928–9933.
16. Kumthip, K., Chusri, P., Jilg, N., Zhao, L., Fusco, D.N., Zhao, H., Goto, K., Cheng, D., Schaefer, E.A., Zhang, L., et al. (2012). Hepatitis C virus NS5A disrupts STAT1 phosphorylation and suppresses type I interferon signaling. J. Virol. *86*, 8581–8591.
17. Takeuchi, K., Kadota, S.I., Takeda, M., Miyajima, N., and Nagata, K. (2003). Measles virus V protein blocks interferon (IFN)-α/β but not IFN-γ signaling by inhibiting STAT1 and STAT2 phosphorylation. FEBS Lett. *545*, 177–182.
18. Mace, T.A., Ameen, Z., Collins, A., Wojcik, S., Mair, M., Young, G.S., Fuchs, J.R., Eubank, T.D., Frankel, W.L., Bekaii-Saab, T., et al. (2013). Pancreatic cancer-associated stellate cells promote differentiation of myeloid-derived suppressor cells in a STAT3-dependent manner. Cancer Res. *73*, 3007–3018.
19. Chaudhry, A., Rudra, D., Treuting, P., Samstein, R.M., Liang, Y., Kas, A., and Rudensky, A.Y. (2009). CD4+ regulatory T cells control TH17 responses in a Stat3-dependent manner. Science *326*, 986–991.
20. Yang, X.O., Panopoulos, A.D., Nurieva, R., Chang, S.H., Wang, D., Watowich, S.S., and Dong, C. (2007). STAT3 regulates cytokine-mediated generation of inflammatory helper T cells. J. Biol. Chem. *282*, 9358–9363.
21. Johnson, D.E., O'Keefe, R.A., and Grandis, J.R. (2018). Targeting the IL-6/JAK/STAT3 signalling axis in cancer. Nat. Rev. Clin. Oncol. *15*, 234–248.
22. Kuchipudi, S.V. (2015). The Complex Role of STAT3 in Viral Infections. J. Immunol. Res. *2015*, 272359.
23. Andrejeva, G., and Rathmell, J.C. (2017). Similarities and Distinctions of Cancer and Immune Metabolism in Inflammation and Tumors. Cell Metab. *26*, 49–70.

24. Chang, C.H., Qiu, J., O'Sullivan, D., Buck, M.D., Noguchi, T., Curtis, J.D., Chen, Q., Gindin, M., Gubin, M.M., van der Windt, G.J., et al. (2015). Metabolic Competition in the Tumor Microenvironment Is a Driver of Cancer Progression. Cell *162*, 1229–1241.

25. Hornyák, L., Dobos, N., Koncz, G., Karányi, Z., Páll, D., Szabó, Z., Halmos, G., and Székvölgyi, L. (2018). The Role of Indoleamine-2,3-Dioxygenase in Cancer Development, Diagnostics, and Therapy. Front. Immunol. *9*, 151.

26. Munn, D.H., and Mellor, A.L. (2016). IDO in the Tumor Microenvironment: Inflammation, Counter-Regulation, and Tolerance. Trends Immunol. *37*, 193–207.

27. Yan, Y., Zhang, G.X., Gran, B., Fallarino, F., Yu, S., Li, H., Cullimore, M.L., Rostami, A., and Xu, H. (2010). IDO upregulates regulatory T cells via tryptophan catabolite and suppresses encephalitogenic T cell responses in experimental autoimmune encephalomyelitis. J. Immunol. *185*, 5953–5961.

28. Munn, D.H., and Mellor, A.L. (2013). Indoleamine 2,3 dioxygenase and metabolic control of immune responses. Trends Immunol. *34*, 137–143.

29. Larrea, E., Riezu-Boj, J.I., Gil-Guerrero, L., Casares, N., Aldabe, R., Sarobe, P., Civeira, M.P., Heeney, J.L., Rollier, C., Verstrepen, B., et al. (2007). Upregulation of indoleamine 2,3-dioxygenase in hepatitis C virus infection. J. Virol. *81*, 3662–3666.

30. Chen, A., Zhang, Y., Meng, G., Jiang, D., Zhang, H., Zheng, M., Xia, M., Jiang, A., Wu, J., Beltinger, C., and Wei, J. (2017). Oncolytic measles virus enhances antitumour responses of adoptive $CD8^{+}NKG2D^{+}$ cells in hepatocellular carcinoma treatment. Sci. Rep. *7*, 5170.

31. Vacchelli, E., Aranda, F., Eggermont, A., Sautès-Fridman, C., Tartour, E., Kennedy, E.P., Platten, M., Zitvogel, L., Kroemer, G., and Galluzzi, L. (2014). Trial watch: IDO inhibitors in cancer therapy. OncoImmunology *3*, e957994.

32. Gandhi, V., and Plunkett, W. (2002). Cellular and clinical pharmacology of fludarabine. Clin. Pharmacokinet. *41*, 93–103.

33. Frank, D.A., Mahajan, S., and Ritz, J. (1999). Fludarabine-induced immunosuppression is associated with inhibition of STAT1 signaling. Nat. Med. *5*, 444–447.

34. Hanafi, L.A., Gauchat, D., Godin-Ethier, J., Possamaï, D., Duvignaud, J.B., Leclerc, D., Grandvaux, N., and Lapointe, R. (2014). Fludarabine downregulates indoleamine 2,3-dioxygenase in tumors via a proteasome-mediated degradation mechanism. PLoS ONE *9*, e99211.

35. Ninomiya, S., Narala, N., Huye, L., Yagyu, S., Savoldo, B., Dotti, G., Heslop, H.E., Brenner, M.K., Rooney, C.M., and Ramos, C.A. (2015). Tumor indoleamine 2,3-dioxygenase (IDO) inhibits CD19-CAR T cells and is downregulated by lymphodepleting drugs. Blood *125*, 3905–3916.

36. Ungerechts, G., Springfeld, C., Frenzke, M.E., Lampe, J., Johnston, P.B., Parker, W.B., Sorscher, E.J., and Cattaneo, R. (2007). Lymphoma chemovirotherapy: CD20-targeted and convertase-armed measles virus can synergize with fludarabine. Cancer Res. *67*, 10939–10947.

37. Meng, G., Xia, M., Wang, D., Chen, A., Wang, Y., Wang, H., Yu, D., and Wei, J. (2014). Mitophagy promotes replication of oncolytic Newcastle disease virus by blocking intrinsic apoptosis in lung cancer cells. Oncotarget *5*, 6365–6374.

38. Horvath, C.M., and Darnell, J.E., Jr. (1996). The antiviral state induced by alpha interferon and gamma interferon requires transcriptionally active Stat1 protein. J. Virol. *70*, 647–650.

39. Dupuis, S., Jouanguy, E., Al-Hajjar, S., Fieschi, C., Al-Mohsen, I.Z., Al-Jumaah, S., Yang, K., Chapgier, A., Eidenschenk, C., Eid, P., et al. (2003). Impaired response to interferon-alpha/beta and lethal viral disease in human STAT1 deficiency. Nat. Genet. *33*, 388–391.

40. Schirrmacher, V. (2015). Signaling through RIG-I and type I interferon receptor: Immune activation by Newcastle disease virus in man versus immune evasion by Ebola virus (Review). Int. J. Mol. Med. *36*, 3–10.

41. Liu, Y., Goulet, M.L., Sze, A., Hadj, S.B., Belgnaoui, S.M., Lababidi, R.R., Zheng, C., Fritz, J.H., Olagnier, D., and Lin, R. (2016). RIG-I-Mediated STING Upregulation Restricts Herpes Simplex Virus 1 Infection. J. Virol. *90*, 9406–9419.

42. Lin, W., Choe, W.H., Hiasa, Y., Kamegaya, Y., Blackard, J.T., Schmidt, E.V., and Chung, R.T. (2005). Hepatitis C virus expression suppresses interferon signaling by degrading STAT1. Gastroenterology *128*, 1034–1041.

43. Munn, D.H., and Bronte, V. (2016). Immune suppressive mechanisms in the tumor microenvironment. Curr. Opin. Immunol. *39*, 1–6.

44. Selvendiran, K., Koga, H., Ueno, T., Yoshida, T., Maeyama, M., Torimura, T., Yano, H., Kojiro, M., and Sata, M. (2006). Luteolin promotes degradation in signal transducer and activator of transcription 3 in human hepatoma cells: an implication for the antitumor potential of flavonoids. Cancer Res. *66*, 4826–4834.

45. Nie, X.H., Ou-yang, J., Xing, Y., Li, D.Y., Dong, X.Y., Liu, R.E., and Xu, R.X. (2015). Paeoniflorin inhibits human glioma cells via STAT3 degradation by the ubiquitin-proteasome pathway. Drug Des. Devel. Ther. *9*, 5611–5622.

46. Ulane, C.M., Rodriguez, J.J., Parisien, J.P., and Horvath, C.M. (2003). STAT3 ubiquitylation and degradation by mumps virus suppress cytokine and oncogene signaling. J. Virol. *77*, 6385–6393.

47. Daino, H., Matsumura, I., Takada, K., Odajima, J., Tanaka, H., Ueda, S., Shibayama, H., Ikeda, H., Hibi, M., Machii, T., et al. (2000). Induction of apoptosis by extracellular ubiquitin in human hematopoietic cells: possible involvement of STAT3 degradation by proteasome pathway in interleukin 6-dependent hematopoietic cells. Blood *95*, 2577–2585.

48. Mao, R., Zhang, J., Jiang, D., Cai, D., Levy, J.M., Cuconati, A., Block, T.M., Guo, J.T., and Guo, H. (2011). Indoleamine 2,3-dioxygenase mediates the antiviral effect of gamma interferon against hepatitis B virus in human hepatocyte-derived cells. J. Virol. *85*, 1048–1057.

49. Jarahian, M., Watzl, C., Fournier, P., Arnold, A., Djandji, D., Zahedi, S., Cerwenka, A., Paschen, A., Schirrmacher, V., and Momburg, F. (2009). Activation of natural killer cells by newcastle disease virus hemagglutinin-neuraminidase. J. Virol. *83*, 8108–8121.

50. Holmgaard, R.B., Zamarin, D., Li, Y., Gasmi, B., Munn, D.H., Allison, J.P., Merghoub, T., and Wolchok, J.D. (2015). Tumor-Expressed IDO Recruits and Activates MDSCs in a Treg-Dependent Manner. Cell Rep. *13*, 412–424.